Article

Cell Reports

Hoxa2 Selects Barrelette Neuron Identity and Connectivity in the Mouse Somatosensory Brainstem

Graphical Abstract

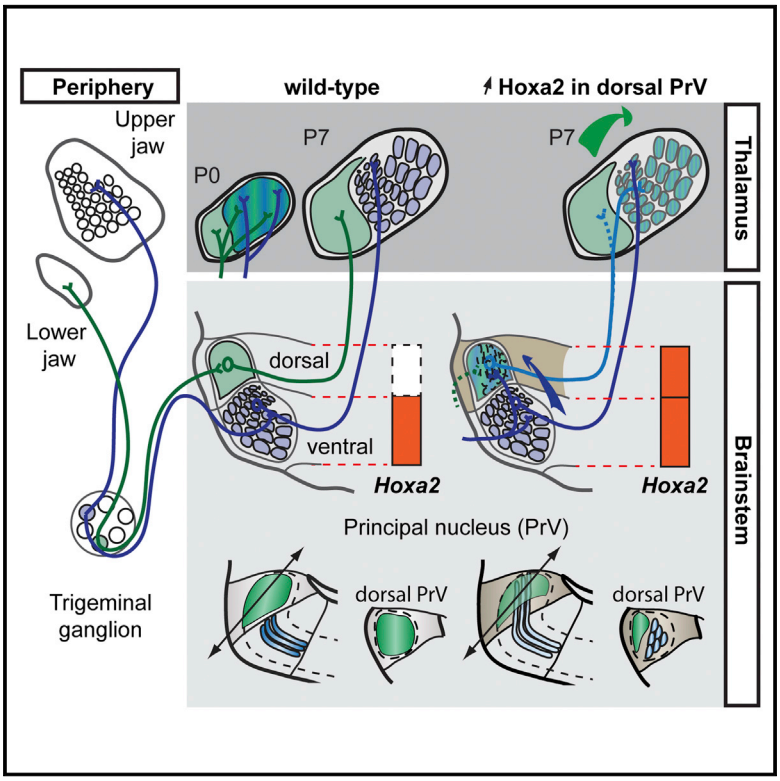

Authors

Ahmad Bechara, Christophe Laumonnerie, Nathalie Vilain, ..., Moritz A. Kirschmann, Sebastien Ducret, Filippo M. Rijli

Correspondence

filippo.rijli@fmi.ch

In Brief

Mouse whiskers are mapped in brainstem nuclei as neuronal modules known as barrelettes. Little is known about how barrelette circuitry is established. Bechara et al. show that *Hoxa2* ectopic expression in dorsal principal nucleus neurons is sufficient to coordinate their topographic input-output connectivity and generate an ectopic barrelette map.

Highlights

- How whisker-related barrelette topography is established is poorly understood
- *Hoxa2* expression in principal neurons is sufficient for barrelette map formation
- *Hoxa2*-expressing principal neurons provide an axon template for the barreloid map
- *Ezh2*-mediated *Hoxa2* repression allows mandibular circuit formation

Bechara et al., 2015, Cell Reports *13*, 783–797
October 27, 2015 ©2015 The Authors
http://dx.doi.org/10.1016/j.celrep.2015.09.031

Cell Reports
Article

Hoxa2 Selects Barrelette Neuron Identity and Connectivity in the Mouse Somatosensory Brainstem

Ahmad Bechara,[1] Christophe Laumonnerie,[1,3] Nathalie Vilain,[1] Claudius F. Kratochwil,[1,4] Vanja Cankovic,[1] Nicola A. Maiorano,[1] Moritz A. Kirschmann,[1] Sebastien Ducret,[1] and Filippo M. Rijli[1,2,*]
[1]Friedrich Miescher Institute for Biomedical Research, Maulbeerstrasse 66, 4058 Basel, Switzerland
[2]University of Basel, 4056 Basel, Switzerland
[3]Present address: St. Jude Children's Research Hospital, 262 Danny Thomas Place, Memphis, TN 38105, USA
[4]Present address: University of Konstanz, Department of Biology, Universitätsstr. 10, D-78457 Konstanz, Germany
*Correspondence: filippo.rijli@fmi.ch
http://dx.doi.org/10.1016/j.celrep.2015.09.031

SUMMARY

Mouse whiskers are somatotopically mapped in brainstem trigeminal nuclei as neuronal modules known as barrelettes. Whisker-related afferents form barrelettes in ventral principal sensory (vPrV) nucleus, whereas mandibular input targets dorsal PrV (dPrV). How barrelette neuron identity and circuitry is established is poorly understood. We found that ectopic *Hoxa2* expression in dPrV neurons is sufficient to attract whisker-related afferents, induce asymmetrical dendrite arbors, and allow ectopic barrelette map formation. Moreover, the thalamic area forming whisker-related barreloids is prenatally targeted by both vPrV and dPrV axons followed by perinatal large-scale pruning of dPrV axons and refinement of vPrV barrelette input. Ectopic *Hoxa2* expression allows topographically directed targeting and refinement of dPrV axons with vPrV axons into a single whisker-related barreloid map. Thus, a single HOX transcription factor is sufficient to switch dPrV into a vPrV barrelette neuron program and coordinate input-output topographic connectivity of a dermatome-specific circuit module.

INTRODUCTION

Facial somatosensory input is wired to the brain through the trigeminal circuit (reviewed in Erzurumlu and Gaspar, 2012; Erzurumlu et al., 2010; O'Leary et al., 1994; Pouchelon et al., 2012) (Figure 1). Facial dermatomes are topographically connected to the brainstem through the peripheral and central axons of trigeminal ganglion (TG) primary sensory neurons that segregate into mandibular, maxillary, and ophthalmic trigeminal nerve branches. Central afferent axons enter the brainstem, make collaterals, and target second order neurons in the principal (PrV) and spinal (SpV) trigeminal nuclei. PrV neurons project contralaterally through the lemniscal pathway to third order neurons in the ventral posterior medial (VPM) thalamus, which in turn innervate the S1 somatosensory cortex area hosting the representation of orofacial structures.

A large portion of the mouse facial representation is devoted to the mystacial vibrissae (whiskers), organized in five rows of four to seven follicles on the snout. Whiskers are mapped as spatially ordered neuronal modules at brainstem (known as barrelettes), thalamic (barreloids), and cortical (barrels) levels faithfully reproducing the whisker spatial arrangement on the face (Ma and Woolsey, 1984; Van Der Loos, 1976; Woolsey and Van der Loos, 1970). Mouse strains with supernumerary whiskers display additional whisker-related modules in the barrel cortex (Ozeki and Tabata, 2002; Van der Loos et al., 1984), suggesting an instructive role of the periphery in imposing a central somatotopic pattern (da Silva et al., 2011; Hodge et al., 2007). On the other hand, a whisker-related matching central pattern might only be induced in intrinsically specified neuronal subsets. At the brainstem level, little is known about PrV intrinsic determinants establishing the post-synaptic barrelette pattern and providing a topographic axonal template for barreloid formation in the thalamus.

Dorsal PrV (dPrV) and ventral PrV (vPrV) are composed of spatially segregated neuronal sub-populations derived from distinct rostrocaudal progenitor compartments, the rhombomere (r)2 and r3 (Oury et al., 2006), respectively. The trigeminal nerve mandibular branch sends collaterals selectively to dPrV, whereas vPrV is targeted by whisker-related afferents of the maxillary branch and forms the barrelette map (reviewed in Erzurumlu et al., 2010). A few transcription factors have been involved in PrV development (Ding et al., 2003; reviewed in Erzurumlu et al., 2010) but to date no single transcription factor nor molecule has been shown to be sufficient on its own to instruct vPrV-specific barrelette neuron sub-type identity and its topographic connectivity. *Hoxa2* expression is differentially maintained in vPrV, although not dPrV, postmitotic progeny (Oury et al., 2006) (Figures S1A–S1L). Moreover, *Hoxa2* is not expressed in the facial mesenchyme nor TG primary neurons (Oury et al., 2006). Thus, *Hoxa2* is a good candidate to specify

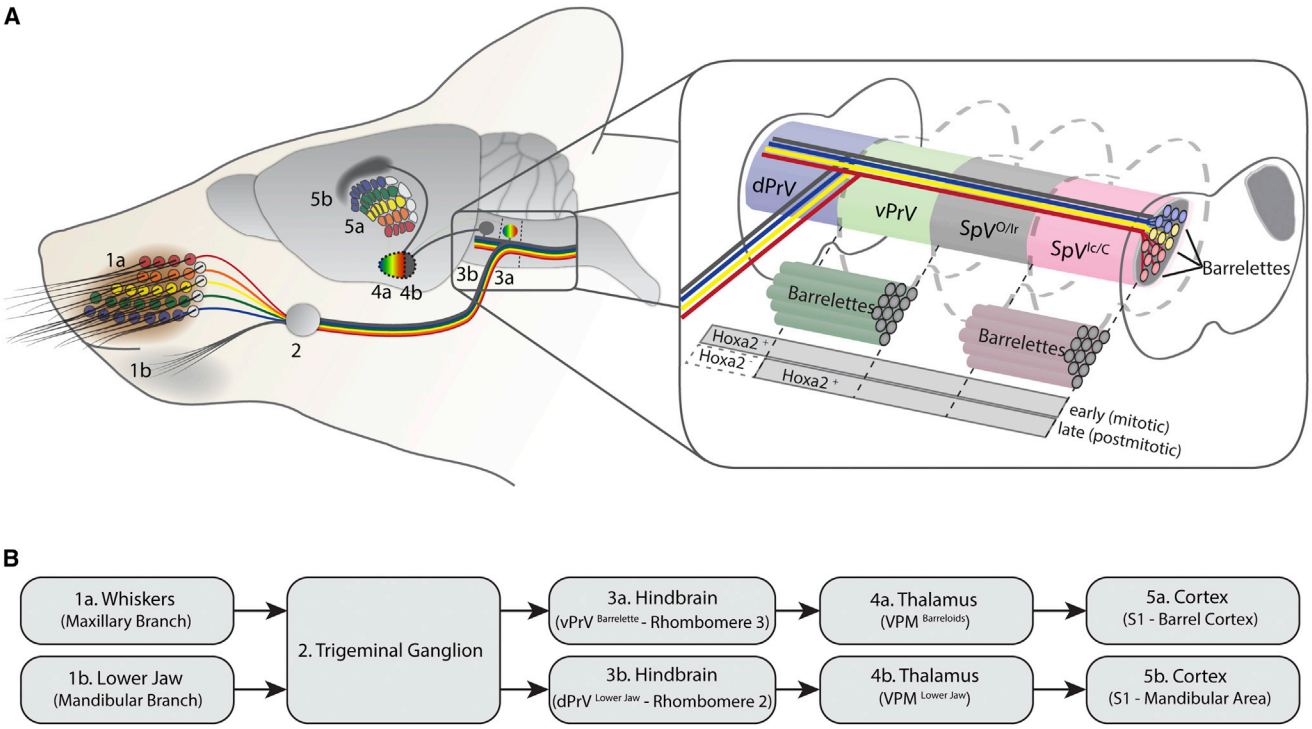

Figure 1. Trigeminal Circuit in the Mouse

(A) Trigeminal circuit diagram in the mouse. The inset shows the brainstem trigeminal nuclear complex and its subdivisions. Barrelettes are formed in vPrV and specific SpV subnuclei. *Hoxa2* is expressed rostrocaudally up to the dPrV mitotic progenitor domain, but not maintained in dPrV, unlike vPrV, postmitotic neurons.

(B) Legend describing each component of the trigeminal circuit. dPrV, dorsal principal trigeminal nucleus; vPrV, ventral principal trigeminal nucleus; SpVo, spinal nucleus, oralis division; SpVir, spinal nucleus, rostral part of interpolaris division; SpVic, spinal nucleus, caudal part of interpolaris division; SpVc, spinal nucleus, caudalis division.

See also Figure S7.

a vPrV barrelette neuron subtype identity and connectivity program. However, *Hoxa2* conditional deletion in r3-derived vPrV neurons resulted in lack of whisker-related primary sensory afferent input to vPrV (Oury et al., 2006), preventing the study of its potential involvement during barrelette map formation.

Here, we found that ectopic maintenance of *Hoxa2* expression in r2-derived dPrV neurons is sufficient to ectopically attract whisker-related primary sensory afferents at the expense of mandibular afferents and results in vPrV-like asymmetrical dendrite arbors in dPrV neurons and ectopic barrelette map formation. Moreover, we show that in wild-type animals the thalamic prenatal barreloid area receives overlapping inputs from both vPrV and dPrV axons; in turn, the infraorbital nerve (ION) relaying whisker input is required to drive perinatal large-scale mandibular dPrV axon terminal pruning, resulting in postnatal maintenance of only vPrV whisker-related barrelette input and barreloid formation. *Hoxa2* expression in dPrV neurons is sufficient to drive topographically directed dPrV axon targeting to the barreloid forming dorsal VPM thalamus, where they are maintained postnatally and refine with vPrV axons into a single barreloid map. Furthermore, *Hoxa2* expression in postmitotic neurons is sufficient to drive the above changes in dPrV neurons. Finally, we show that *Ezh2* is normally required for epigenetic repression of *Hoxa2* in postmitotic dPrV neurons, thus preventing barrelette circuit formation and allowing mandibular circuit development. *Hoxa2* is therefore a key gene able to switch dPrV to vPrV barrelette neuron subtype identity and orchestrating topographic barrelette connectivity and map formation.

RESULTS

Hoxa2 Expression Is Maintained in Barrelette but Not dPrV Postmitotic Neurons

To analyze *Hoxa2* expression during early PrV development, we carried out in situ hybridization on adjacent coronal sections at E10.5 (Figures S1A–S1F) and E11.5 (Figures S1G–S1L) using antisense probes for *Hoxa2* and the postmitotic marker *Drg11* (Ding et al., 2003). In the brainstem trigeminal sensory column, *Drg11* is expressed in postmitotic cells of the developing PrV, as well as in the SpV pars oralis (SpVo) and pars caudalis (SpVc) that do not project to VPM, but not in the SpV pars interpolaris (SpVi), and its expression is maintained throughout prenatal and postnatal stages (Ding et al., 2003). At E10.5, *Drg11*$^{+}$ postmitotic cells first emerged from the ventricular zone of presumptive dPrV (Figure S1A) and vPrV (Figure S1D) (Ding et al., 2003). *Hoxa2* expression was present in both dPrV and vPrV

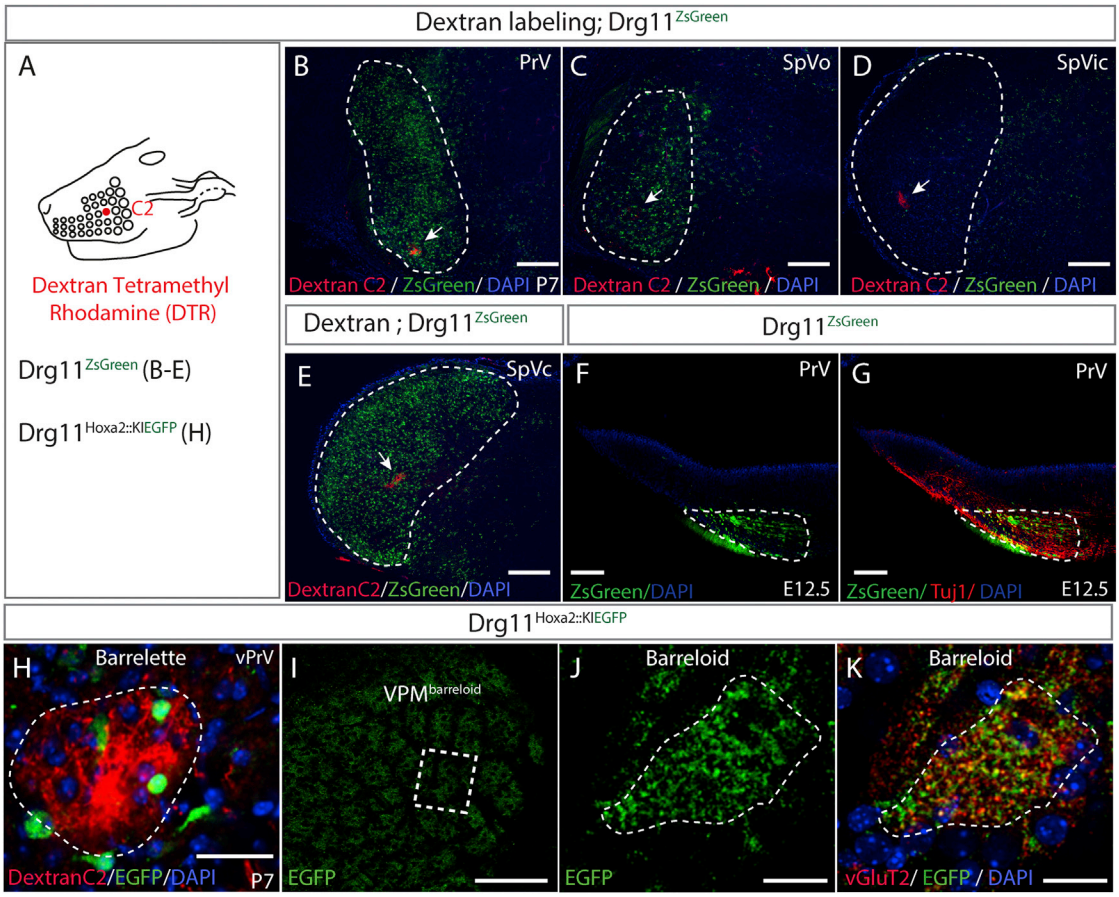

Figure 2. *Hoxa2* Expression in PrV Barrelette Neurons

(A) Drawing illustrating C2 whisker afferent labeling by dextran injection and legend referring to corresponding experimental panels.

(B–E) ZsGreen immunostaining in P7 *Drg11*^{zsGreen} mice showing PrV, SpVo, and SpVc, but not SpVic, trigeminal nuclei labeling. Trigeminal subdivisions identified by dextran-labeled C2 afferents targeting (red). Input detected in ventral PrV (barrelette-like) but not dorsal PrV (B), SpVo (sparse) (C), SpVic (barrelette-like) (D), and SpVc (barrelette-like) (E). Scale bars, 200 μm.

(F and G) Coronal sections through E12.5 PrV of *Drg11*^{ZsGreen} mouse. Anti-ZsGreen (green) and anti-Tuj1 neuronal marker immunostainings show *Drg11*-driven Cre-mediated recombination only in postmitotic neurons. DAPI stains cell nuclei. Scale bars, 100 μm.

(H) Coronal section through a P7 barrelette in *Drg11*$^{Hoxa2::KIEGFP}$ vPrV. Dextran-labeled C2 whisker primary afferents (red) are surrounded by *Hoxa2*-driven *EGFP*-expressing barrelette cells (green). *Hoxa2*-dependent *EGFP* expression was induced upon *Drg11*-driven Cre-mediated excision. Scale bar, 20 μm.

(I–K) Coronal section through dorsal VPM thalamus in P7 *Drg11*$^{Hoxa2::KIEGFP}$ animal. The barreloid map is visualized by *EGFP*$^{+}$ axon terminals (green) (I) from the *Hoxa2*-expressing barrelette cells in (H). (J and K) Magnified barreloid showing overlapping (yellow, merge in K) of Hoxa2^{+}/EGFP^{+} (green) (J) and vGluT2^{+} (red) presynaptic terminals. PrV, principal trigeminal nucleus; SpVo, spinal nucleus, oralis division; SpVic, spinal nucleus, caudal part of interpolaris division; SpVc, spinal nucleus, caudalis division; VPM, ventral posterior medial nucleus. Scale bars, 100 μm (I), 20 μm (J and K).

See also Figure S1.

progenitor domains, albeit with lower levels in dPrV, but only maintained in *Drg11*$^{+}$ vPrV postmitotic cells whereas it was silenced in *Drg11*$^{+}$ dPrV cells (compare Figures S1B and S1C and S1E and S1F, and S1H and S1I and S1K and S1L).

To map *Hoxa2* expression in *Drg11*-expressing barrelette neurons in vPrV we used a genetic intersectional strategy. We generated a *Drg11::Cre* BAC transgenic line and crossed it with the Cre-inducible reporter lines *R26R*^{lacZ} (Soriano, 1999) (hereafter referred to as *Drg11*^{lacZ}) and *R26R*^{ZsGreen} (referred to as *Drg11*^{ZsGreen}). The reporter expression reproduced, albeit with some mosaicism, the endogenous *Drg11* expression pattern (Figures 2B–2E and S2A–S2D). In the brainstem, the distinct dPrV, vPrV, SpVo, and SpVc *Drg11*$^{+}$ subnuclei were further identified at P7 based on the targeting pattern of single (C2) whisker-related, dextran-labeled, primary afferents. Namely, vPrV and SpVc *Drg11*^{ZsGreen} neurons were targeted by C2 collaterals organized in a barrelette pattern whereas dPrV *Drg11*^{ZsGreen} neurons did not receive whisker-related input (Figures 2B–2E), and SpVo only sparse C2-related collaterals (Figure 2C). The SpVi caudal part (SpVic), as mapped by the C2 barrelette, did not contain *Drg11*^{ZsGreen} neurons (Figure 2D). Importantly, *ZsGreen*$^{+}$ or *LacZ*$^{+}$ cells were only present in postmitotic neurons and never found at any stage in the progenitor domain, as assessed by co-staining with the postmitotic neuronal marker TUJ1

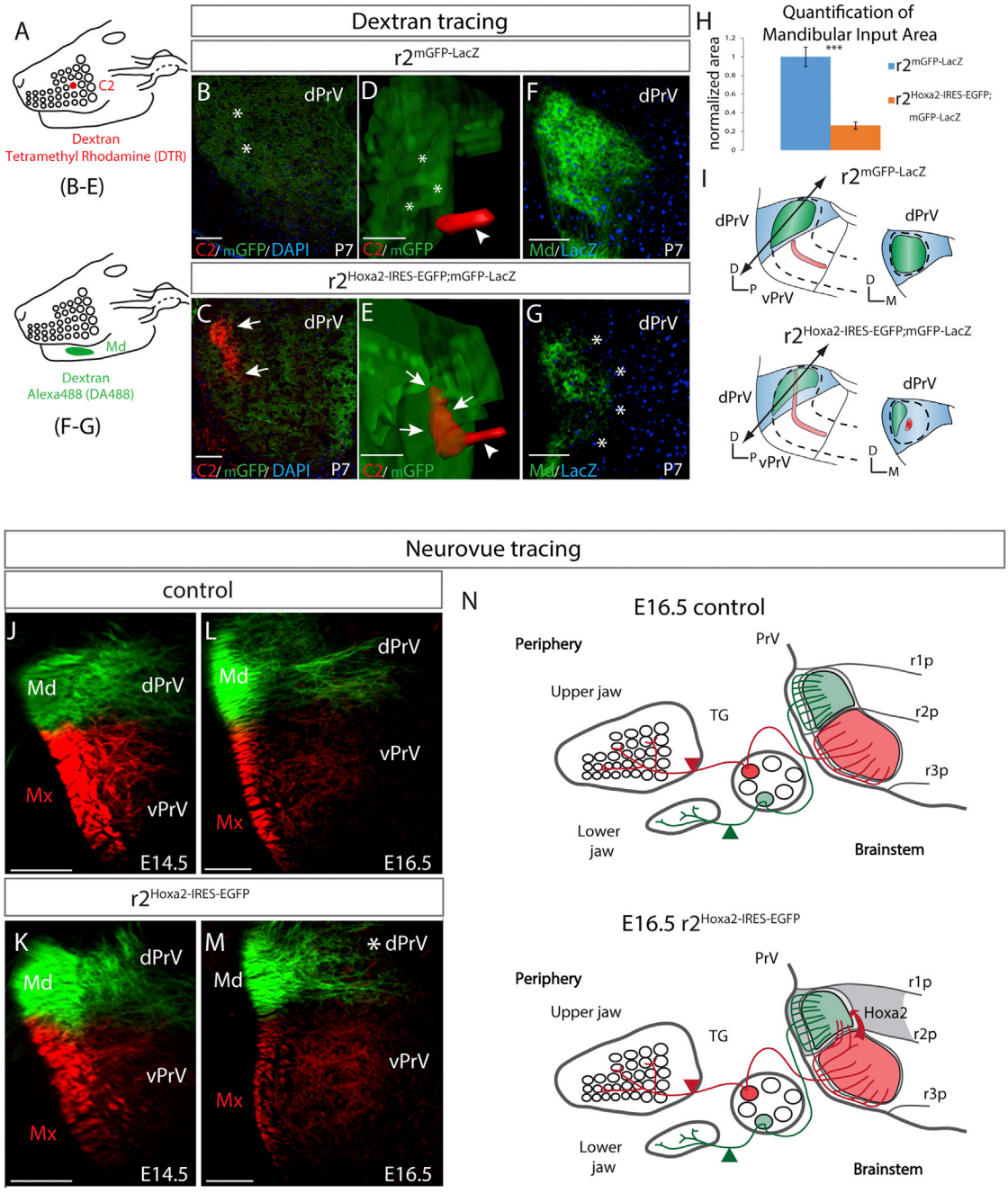

Figure 3. *Hoxa2* Expression in Dorsal PrV Attracts Whisker-specific Afferents at Late Prenatal Stage at the Expense of Mandibular Input

(A) Drawings illustrating DTR injections to label C2 whisker (red) and dextran Alexa488 (DA488) injections to label mandibular (green) afferents. Legend refers to experimental panels; dextran labeling is detected by direct fluorescence.

(B and C) dPrV coronal sections immunostained for mGFP (green) showing ectopic barrelette-like input by C2 whisker dextran-labeled afferents (arrows, red) in (C); no input (asterisks) is present in controls (B). P7 $r2^{mGFP\text{-}lacZ}$ mice (B). $r2^{Hoxa2\text{-}IRES\text{-}EGFP;mGFP\text{-}lacZ}$ mice (C). Scale bars, 100 μm.

(D and E) PrV section 3D reconstruction showing ectopic barrette-like C2 whisker dextran-labeled afferents (red, arrows) into dPrV immunostained for mGFP (green) in (E), co-extensive with the vPrV C2 barrelette (arrowhead), as compared to (D). P7 $r2^{mGFP\text{-}lacZ}$ mice (D). $r2^{Hoxa2\text{-}IRES\text{-}EGFP;mGFP\text{-}lacZ}$ mice (E). Scale bars, 200 μm.

(F–H) Mandibular (Md) dextran-labeled afferents target dPrV (LacZ staining, blue) in (F), whereas Md input is much reduced (asterisks) in (G); quantification in (H). In (F) and (G), discrimination between green dextran and mGFP signals is achieved as dextran labeling provides a bright and spatially restricted signal in direct fluorescence, whereas the mGFP signal can only be detected by antibody staining in these mice. The extent of r2-derived dPrV territory is detected by Xgal staining (blue). P7 $r2^{mGFP\text{-}lacZ}$ mice (F). $r2^{Hoxa2\text{-}IRES\text{-}EGFP;mGFP\text{-}lacZ}$ mice (G). Scale bars, 100 μm.

(I) Summary drawing of findings in (B)–(H).

(legend continued on next page)

(Figures 2F and 2G). We next crossed *Drg11::Cre* with the *Hoxa2*$^{EGFP(lox-neo-lox)}$ knockin allele (Pasqualetti et al., 2002) expressing EGFP from the *Hoxa2* locus upon Cre-mediated recombination (referred to as *Drg11*$^{Hoxa2::KIEGFP}$). In P7 *Drg11*$^{Hoxa2::KIEGFP}$ vPrV, we readily identified individual *Hoxa2/EGFP*$^{+}$ barrelette neurons by their projection to VPM barreloids (Figures 2I–2K) and their innervation by single whisker-related, dextran-labeled, primary afferents (Figure 2H).

Ectopic *Hoxa2* Expression in dPrV Is Sufficient to Generate an Ectopic Barrelette Map at the Expense of Mandibular Input

We then asked whether ectopic maintenance of *Hoxa2* expression in dPrV neurons was sufficient for them to switch to a vPrV-specific barrelette program. To this aim, we conditionally expressed *Hoxa2* by crossing the *r2::Cre* driver (Experimental Procedures; Figures S2I–S2M) (Ren et al., 2002) with the *ROSA::(lox-stop-lox)Hoxa2-IRES-EGFP* knock-in allele (Miguez et al., 2012) (referred to as *r2*$^{Hoxa2\text{-}IRES\text{-}EGFP}$). The *r2::Cre* driver allows Cre-mediated recombination of floxed alleles in r2 mitotic progenitors (Ren et al., 2002) (Figure S2J). When mated to Cre-inducible floxed reporter alleles, as for instance *R26R*^{ZsGreen} (*r2*^{ZsGreen}) or *Tau*$^{(lox\text{-}stop\text{-}lox)mGFP\text{-}IRES\text{-}NLSlacZ}$ (Hippenmeyer et al., 2005) (*r2*$^{mGFP\text{-}lacZ}$), reporter expression is maintained through postnatal stages in the r2-derived postmitotic progeny including dPrV neurons, as assessed by their afferent connectivity and targeting pattern of projections into VPM thalamus (Figures 3, 6, and S2) (Oury et al., 2006), whereas no recombination is observed in the trigeminal ganglion (Figure S2K). Similarly, in *r2*$^{Hoxa2\text{-}IRES\text{-}EGFP}$ mice ectopic *Hoxa2* expression was maintained by the *ROSA* promoter in the postmitotic r2-derived progeny, including dPrV, through postnatal stages as detected by EGFP antibody immunostaining (as a proxy for HOXA2) and *Hoxa2* in situ hybridization (Figures 4D and 5D).

Next, we assessed the targeting patterns of dextran-labeled mandibular and whisker primary sensory afferents into the dPrV of control *r2*$^{mGFP\text{-}lacZ}$ and *r2*$^{Hoxa2\text{-}IRES\text{-}EGFP}$ mice. To identify the r2-derived dPrV territory in *Hoxa2*-expressing mice, we mated *r2*$^{Hoxa2\text{-}IRES\text{-}EGFP}$ to *Tau*$^{(lox\text{-}stop\text{-}lox)mGFP\text{-}IRES\text{-}NLSlacZ}$ (Hippenmeyer et al., 2005) (referred to as *r2*$^{Hoxa2\text{-}IRES\text{-}EGFP;mGFP\text{-}lacZ}$) and either stained for beta-galactosidase or took advantage of the differences in cellular staining between the EGFP from the *Hoxa2-IRES-EGFP* allele and the membrane-expressed GFP from the *mGFP-lacZ* allele. In P7 control *r2*$^{mGFP\text{-}lacZ}$ mice (n = 10), dPrV was targeted by dextran-labeled mandibular (Md) (Figures 3A, 3F, and 3H) although not whisker-specific afferents (Figures 3A, 3B, 3D, and 3I), confirming previous work (Oury et al., 2006). Notably, in P7 *r2*$^{Hoxa2\text{-}IRES\text{-}EGFP;mGFP\text{-}lacZ}$ animals (n = 10) single-whisker (C2) afferent input ectopically innervated the dPrV territory (Figures 3A, 3C, 3E, and 3I), at the expense of Md afferent input that was strongly reduced (compare Figures 3F and 3G and 3I, quantifications in 3H). C2 whisker afferent collaterals were clustered and surrounded by EGFP^{+} cells (Figures 4A and 4D) that provided a postnatal readout of the *Hoxa2-IRES-EGFP* allele expression.

Moreover, simultaneous tracings with distinct fluorescent dextrans of afferents innervating adjacent whiskers in the same (C2 and C3) or distinct (C2 and D2) rows on the mouse face revealed that presynaptic terminals in dPrV of *r2*$^{Hoxa2\text{-}IRES\text{-}EGFP}$ P7 mice segregated into ectopic barrelette-like columns at distinct positions (Figures 4B, 4C, 4E, 4F, and 4K), establishing an ectopic topographic map similar to that normally observed in vPrV (Figures 4G and 4H) and SpV (Figures 4I and 4J). 3D-reconstruction of tissue sections further revealed that the ectopic barrelette columns of whisker-related afferents in dPrV were co-extensive with the vPrV barrelette columns rather than forming an independent duplicated barrelette set (compare Figures 3D and 3E and 4K).

Late Onset of Ectopic Whisker Afferent Input in dPrV of *r2*$^{Hoxa2\text{-}IRES\text{-}EGFP}$ Mice

To address the timing of onset of ectopic whisker afferent targeting of dPrV, we investigated prenatal stages. Unlike at P7, at E14.5 and E16.5 NeuroVue tracing of mandibular (Md) and whisker-related maxillary (Mx) afferents revealed largely normal segregated patterns of collateral targeting in dPrV and vPrV of *r2*$^{Hoxa2\text{-}IRES\text{-}EGFP}$ fetuses (n = 6 per stage), respectively, as compared to wild-type (Figures 3J–3N) (Oury et al., 2006). In two out of six E16.5 *r2*$^{Hoxa2\text{-}IRES\text{-}EGFP}$ fetuses, very few Mx collaterals appeared to have entered the dPrV territory and overlapped with Md input (asterisk, Figure 3M). As the Mx afferent collateral targeting of vPrV neurons occurs with normal schedule (Figures 3J–3M), these findings indicate that it is the late persistence of *Hoxa2* expression in postmitotic dPrV neurons rather than its early overexpression in mitotic progenitors to drive ectopic whisker-related afferent targeting of dPrV (see below, and Figure 6). In further support of this interpretation, Md input appears largely normal up to at least E16.5 (Figures 3K–3M), whereas it is strongly reduced at P7 (Figures 3G–3I).

Thus, the accumulation of ectopic *Hoxa2* expression becomes sufficient to attract the bulk of whisker-related afferents onto dPrV neurons only during late prenatal-early postnatal stages, allowing organization into an ectopic topographic barrelette map.

TVA/EnvA Cell-Specific Viral Tracing and Dendrite Arbor 3D Analysis Reveal Barrelette Neuron-like Features of Ectopic *Hoxa2*-Expressing dPrV Neurons

Next, we wished to assess whether the generation of a whisker afferent map in dPrV would be accompanied by specific changes in post-synaptic dPrV neurons. To this aim, we first carried out in situ hybridization with an antisense probe for *Btbd3*, an activity-dependent factor controlling dendrite asymmetric

(J–M) NeuroVue-labeled maxillary (Mx, red) and Md (green) afferent targeting of dPrV and vPrV at E14.5 (J and K) and E16.5 (L and M) in control (J and L) and *r2*$^{Hoxa2\text{-}IRES\text{-}EGFP}$ (K and M) specimen. Note normal afferent segregation patterns in (J) and (K). Asterisk (M) shows some ectopic Mx collaterals in dPrV. Scale bars, 100 μm.

(N) Summary drawing of findings in (J)–(M). dPrV, dorsal principal trigeminal nucleus; vPrV, ventral principal trigeminal nucleus; r1p-r3p, rhombomere 1–3-derived progeny.

See also Figure S2.

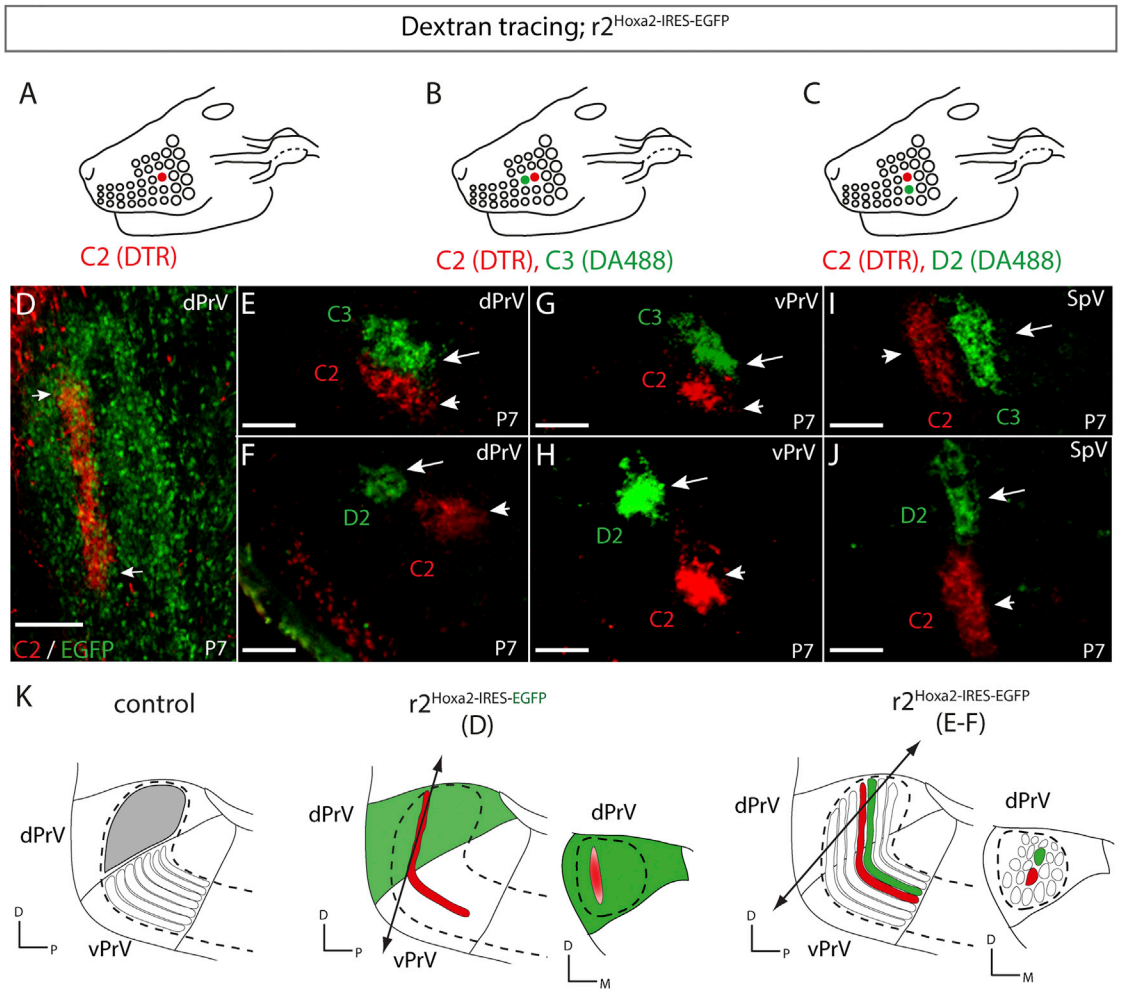

Figure 4. *Hoxa2* Expression in Dorsal PrV Is Sufficient to Generate an Ectopic Topographic Barrelette Map

(A–C) Drawings illustrating dextran injections to trace C2 (A), C2 and C3 (B), and C2 and D2 (C) whisker afferents in P7 $r2^{Hoxa2\text{-}IRES\text{-}EGFP}$ animals. DTR and dextran Alexa488 (DA488) were used to label C2 (red) and C3 and D2 (green) whisker afferents, respectively.

(D–J) Dextran-labeled whisker-specific afferents detected by direct fluorescence targeting dPrV (D–F), vPrV (G–H), and SpV (I–J) in P7 $r2^{Hoxa2\text{-}IRES\text{-}EGFP}$ animals. (D) Oblique section showing ectopic barrelette-like C2 column surrounded by immunostained $EGFP^{+}$ (green, arrows) ectopic *Hoxa2*-expressing cells. (E, G, and I) C2 (red, arrowhead) and C3 (green, arrow), (F, H, and J) C2 (red, arrowhead) and D2 (green, arrow) barrelette-forming afferents in dPrV (ectopic) (E and F), vPrV (G and H), and SpV (I and J). In (E)–(J), discrimination between green dextran and EGFP signals is achieved as dextran labeling provides a bright and spatially restricted signal in direct fluorescence, whereas the EGFP signal can only be detected by antibody staining in these mice (D). Scale bars, 100 μm (D), 50 μm (E–J).

(K) Summary drawing showing ectopic barrelette map formation (red or red and green) upon ectopic *Hoxa2* expression in r2-derived dPrV neurons. Legends refer to experimental panels. dPrV, dorsal principal trigeminal nucleus; vPrV, ventral principal trigeminal nucleus; SpV, spinal trigeminal nucleus.

See also Figure S2.

orientation and remodeling during formation of cortical barrels (Matsui et al., 2013). Interestingly, we found that in control P3 animals *Btbd3* is expressed at the brainstem level in vPrV, although not SpV, barrelettes (Figures 5G and 5I) suggesting PrV versus SpV-specific rostrocaudal differences along the brainstem trigeminal column in the molecular programs of barrelette neuron subtypes. In dPrV, as identified by *Drg11* and lack of *Hoxa2* expression on adjacent sections (Figures 5A and 5C), *Btbd3* transcript distribution appeared diffuse and not clearly organized in neuronal modules as in vPrV (Figure 5E). Notably, in the $r2^{Hoxa2\text{-}IRES\text{-}EGFP}$ dPrV (n = 6) (Figures 5B and 5D) *Btbd3* transcripts appeared to be organized in an ectopic barrelette-like pattern (compare Figures 5E and 5F), suggesting barrelette-like dendrite changes in dPrV neurons.

We therefore compared the dendrite patterns of VPM-projecting vPrV barrelette and dPrV neurons in control and ectopic *Hoxa2* expressing mice (Figures 5K–5R and S3A–S3L). To trace vPrV barrelette neurons, we stereotaxically injected the SAD-ΔG-mCherry rabies virus (Osakada et al., 2011) in dorsal VPM of P8 wild-type mice and analyzed retrogradely labeled barrelette neurons in vPrV at P12. Infected neurons expressed mCherry allowing 3D morphometric analysis of their dendrite arbors. Barrelette neurons displayed dendrites with short branches asymmetrically oriented toward the barrelette hollow

(Figures 5O–5R and S3I–S3L), confirming previous work (Lee et al., 2005).

Both vPrV and dPrV neurons project to the VPM thalamus (Oury et al., 2006; reviewed in Erzurumlu et al., 2010; see below). To selectively retrogradely trace only r2-derived dPrV projecting neurons, we used the TVA/EnvA cell-type-specific viral infection system (Beier et al., 2011; Osakada and Callaway, 2013) and generated *r2::Cre;LSL-R26*$^{TVA\text{-}lacZ}$ (referred to as *r2*$^{TVA\text{-}lacZ}$) and *r2*$^{Hoxa2\text{-}IRES\text{-}EGFP}$*;LSL-R26*$^{TVA\text{-}lacZ}$ (*r2*$^{Hoxa2\text{-}IRES\text{-}EGFP;TVA\text{-}lacZ}$) mice. Following injection of the EnvA-pseudotyped G-deleted mCherry rabies virus in the P8 *r2*$^{TVA\text{-}lacZ}$ VPM, only the axons of r2-derived TVA-expressing VPM-projecting neurons were selectively infected. At P12, the vast majority of retrogradely mCherry-labeled TVA-expressing neurons within the r2-derived territory were localized in dPrV (Figures S4A–S4C) and displayed dendrites with a wide range of branch orientations and longer lengths than barrelette neurons (Figures 5K, 5L, 5Q, 5R, and S3A–S3D). Notably, the dendrite arbors of VPM-projecting neurons in *r2*$^{Hoxa2\text{-}IRES\text{-}EGFP;TVA\text{-}LacZ}$ mice appeared "barrelette-like" i.e., relatively short and asymmetrically oriented (Figures 5M, 5N, 5Q, 5R, and S3E–S3H), similar to vPrV barrelette neurons (compare with Figures 5O–5R and S3I–S3L).

Together with the analysis of the targeting patterns of whisker primary sensory afferents (Figures 3 and 4), the latter results show that ectopic *Hoxa2* expression in dPrV neurons is sufficient to orchestrate pre- and post-synaptic changes resulting in the formation of a vPrV-like barrelette map.

ION-Dependent Perinatal Large-Scale Pruning of dPrV Mandibular Axons in the Thalamic Barreloid Area

Analysis of r2-derived dPrV and r3-derived vPrV projection patterns indicated spatial segregation of mandibular (lower jaw) and whisker-related axonal projection zones into postnatal VPM (Oury et al., 2006). To simultaneously visualize dPrV and vPrV axon terminals into VPM, we generated the *r2::mCherry* (referred to as *r2*^{mCherry}) transgenic line (Figures S2E–S2H), expressing the red fluorescent protein mCherry in r2 derivatives, including dPrV neurons (Figure S2G) and axon terminals (Figures 6A, 6C, 6D, and 6F), and crossed it with *Krox20::Cre;Tau*$^{(lox\text{-}stop\text{-}lox)mGFP\text{-}IRES\text{-}NLSlacZ}$ (referred to as *r3*^{mGFP}) mice allowing to trace r3-derived vPrV axon terminals by mGFP expression (Figures 6B, 6C, 6E, 6F, 6O, and 6P). In P7 *r2*^{mCherry}*;r3*^{mGFP} mice, dPrV mCherry$^+$ and vPrV mGFP$^+$ axon terminal distribution in VPM was mutually exclusive (Figures 6F and 6K). vPrV mGFP$^+$ terminals selectively targeted the dorsolateral VPM and clustered in barreloid hollows, whereas dPrV mCherry$^+$ axons mostly targeted the ventromedial VPM including the lower jaw area (VPM^{LJ}) and a dorsolateral domain excluding barreloids and bordering the posterior (PoM) nucleus (Figure 6F), confirming previous work (Oury et al., 2006).

Moreover, sparse mCherry$^+$ terminals in the P7 barreloid area (Figure 6D, arrows; see also Figures 6H and 6L) suggested the presence of remnants of large-scale elimination of mandibular dPrV axon branches from the whisker-related vPrV projection area. At P0, mGFP$^+$ axons selectively projected to the dorsal VPM (Figures 6B, 6C, and 6K), similar to postnatal stages, indicating topographically directed vPrV targeting to the future barreloid area. In contrast, at P0, unlike at P7, dPrV mCherry$^+$ axons targeted the entire VPM dorsoventral extent overlapping with vPrV mGFP$^+$ axons in the future barreloid territory (Figures 6A, 6C, 6K; see also Figures 6G and 6R), despite segregation of dPrV and vPrV neurons at brainstem level (Figure S2G) (Oury et al., 2006). Therefore, most of dPrV projections are eliminated from the future barreloid area at early postnatal stages.

To address whether the maxillary nerve carrying whisker sensory information plays a role in thalamic input pruning, we induced unilateral whisker input deprivation in *r2*$^{mGFP\text{-}lacZ}$ mice by a neonatal (P0) lesion of the infraorbital nerve (ION). ION lesions were carried out immediately at birth, as the bulk of dPrV axon terminals in dorsal VPM were eliminated quite rapidly perinatally. In P7 sensory deprived mice, vPrV vGluT2$^+$ axon terminals contralateral to the lesion targeted the dorsal VPM but were not clustered in barreloid modules (Figures 6I, 6K, and 6P), in keeping with previous work (reviewed in Erzurumlu and Gaspar, 2012). Interestingly, mandibular dPrV mGFP$^+$ axon terminals were not eliminated and overlapped with vPrV vGluT2$^+$ terminals in dorsal VPM (Figures 6J and 6K), unlike in the undeprived side (Figures 6H and 6K).

Thus, in addition to its involvement in the emergence of barreloid pattern, we found that ION-dependent activity and/or retrograde molecular signaling from periphery is required for the elimination of non-vPrV axons from the VPM barreloid area.

Hoxa2 Is Sufficient to Drive Topographically Directed Axon Targeting to the Barreloid Area and Allow ION-Dependent Refinement into a Barreloid Map

We next asked whether *Hoxa2* is sufficient to drive topographically guided PrV axon targeting to the barreloid area. Unlike the normal pattern of dPrV projections (Figures 6D, 6H, 6L, and 6X), in P7 *r2*$^{Hoxa2\text{-}IRES\text{-}EGFP}$ mice the ventromedial lower jaw VPM (VPM^{LJ}) area was mostly devoid of EGFP$^+$ afferents while axon terminals from dPrV *Hoxa2*$^+$ ectopic barrelettes were maintained in dorsal VPM and segregated into barreloids (Figures 6M and 6X). Notably, EGFP$^+$ dPrV axon targeting was mostly spatially restricted to the developing barreloid area already at P0 (Figures 6N and 6X), a pattern similar to the vPrV projections (Figure 6B). In P7 *r2*$^{Hoxa2\text{-}IRES\text{-}EGFP}$ barreloids, we detected both vGluT2$^+$/EGFP$^+$ and vGluT2$^+$/EGFP$^-$ pre-synaptic terminals (Figure 6Q, arrows). NeuroVue anterograde tracings (n = 4) showed that individual barreloids were targeted both by dPrV (arrowhead) and vPrV (arrow) axon terminals (Figures S5D–S5H), unlike in wild-type (n = 4) (Figures S5A–S5C). In *r2*$^{Hoxa2\text{-}IRES\text{-}EGFP}$ animals, clustering of vGluT2$^+$/EGFP$^+$ terminals into barreloid modules was impaired after a neonatal (P0) lesion of the ION (Figures 6N and 6X), indicating that it requires whisker-related activity and/or retrograde molecular signaling from periphery.

Expression of *Hoxa2* in Postmitotic dPrV Neurons Is Sufficient to Induce Barrelette Neuron-like Connectivity

The use of the *r2::Cre* driver allows regional specificity driving *Hoxa2* ectopic expression selectively in r2 derivatives, including dPrV mitotic progenitors and postmitotic neurons. The prenatal analysis suggested that the late persistence of *Hoxa2* expression in postmitotic dPrV neurons through early postnatal stages may be sufficient to drive whisker-related vPrV-like connectivity of

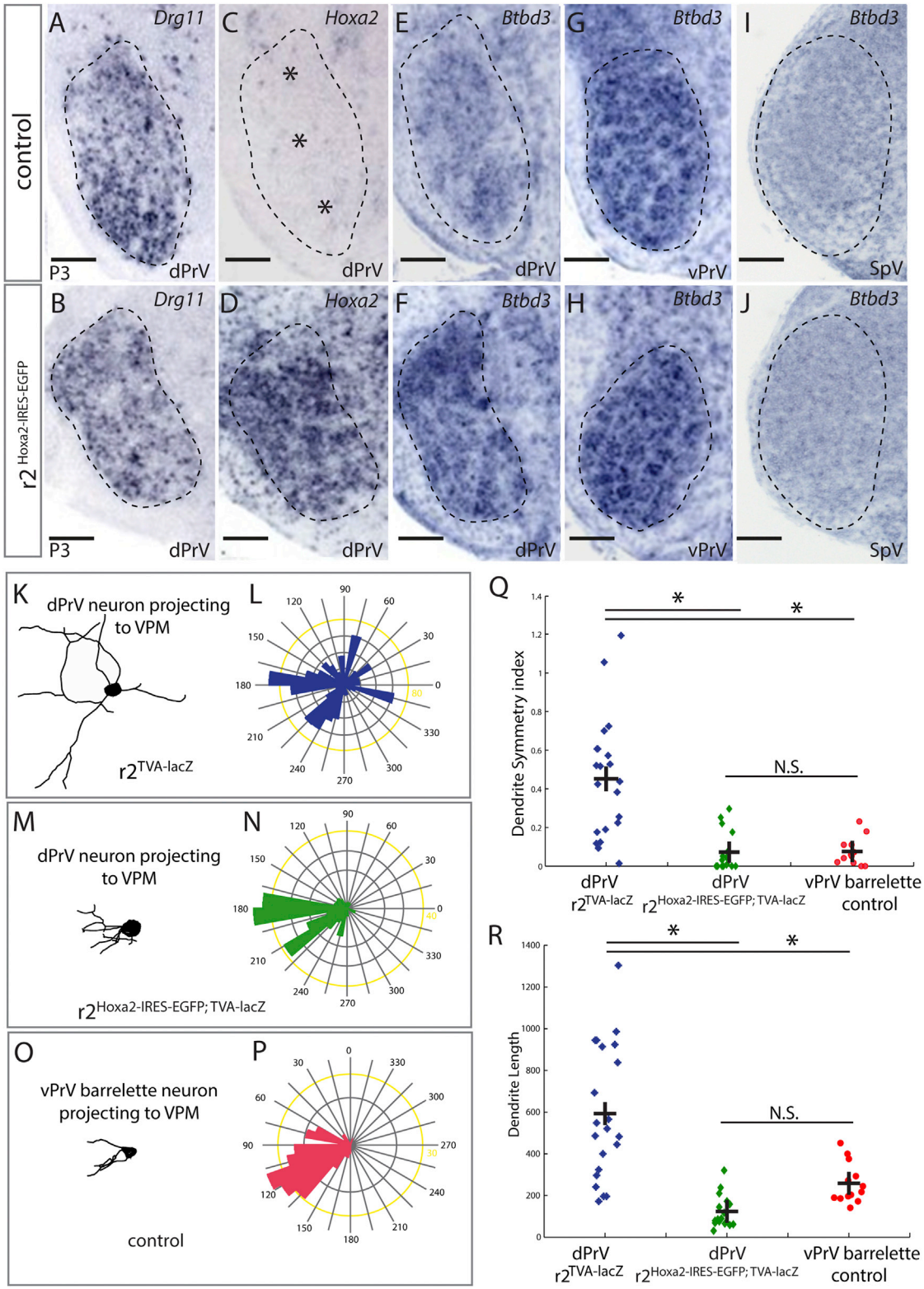

Figure 5. Ectopic *Hoxa2* Results in *Btbd3* Expression and Barrelette-like Dendrite Patterns in dPrV Neurons Projecting to VPM Thalamus

(A–J) In situ hybridization with *Drg11* (A and B), *Hoxa2* (C and D), and *Btbd3* (E–J) antisense probes on coronal sections of dPrV (A–F), vPrV (G and H), and SpV (I and J) in control (A, C, E, G, and I) and $r2^{Hoxa2\text{-}IRES\text{-}EGFP}$ (B, D, F, H, and J) P3 animals. Note barrelette-like patterns of *Btbd3* expression in (G), (H) and (F) although not in (E), (I), and (J). Scale bars, 100 μm.

(legend continued on next page)

dPrV neurons. On the other hand, a caveat is that *Hoxa2* ectopic expression is obtained in a larger cell population than just dPrV neurons, as the *r2::Cre* line does not allow cell specificity.

To achieve postmitotic expression in PrV neurons, we mated the *Drg11::Cre* with the *ROSA::(lox-stop-lox)Hoxa2-IRES-EGFP* allele (referred to as $Drg11^{Hoxa2\text{-}IRES\text{-}EGFP}$). Although the *Drg11::Cre* driver acts on both vPrV and dPrV, the vPrV already expresses *Hoxa2*, so effectively is ectopic only in dPrV. Indeed, in $Drg11^{Hoxa2\text{-}IRES\text{-}EGFP}$ specimen (n = 8), C2 whisker dextran-labeled afferents ectopically innervated the dPrV, unlike in control $Drg11^{ZsGreen}$ mice (Figures 6T and 6X), and segregated in barrelette-like structures (Figures 6V and 6X) similar to $r2^{Hoxa2\text{-}IRES\text{-}EGFP}$ mice (Figures 3C and 4D). The *r2::Cre* line does not drive expression in trigeminal ganglion sensory neurons, unlike the *Drg11::Cre* line (compare Figures S2K and S2B). Thus, these findings strongly indicate that the ectopic barrelette-like clustering of whisker afferents in $Drg11^{Hoxa2\text{-}IRES\text{-}EGFP}$ dPrV is mainly the result of ectopic *Hoxa2* expression in dPrV neurons. Moreover, in the P7 VPM thalamus of $Drg11^{Hoxa2\text{-}IRES\text{-}EGFP}$ mice, very few, if any, $EGFP^+$ axon terminals were found in the lower jaw representation area (Figures 6W and 6X), as compared to $Drg11^{ZsGreen}$ control mice (Figures 6U and 6X). The bulk of $EGFP^+$ afferents targeted the dorsal VPM and segregated into barreloids, similar to $r2^{Hoxa2\text{-}IRES\text{-}EGFP}$ mice (compare Figures 6W and 6M).

In summary, the only expression of *Hoxa2* in postmitotic dPrV neurons is sufficient to induce a barrelette neuron vPrV-like connectivity pattern. These findings complement the results obtained with the *r2::Cre* driver and further support the conclusion that persistent *Hoxa2* postmitotic expression is sufficient to switch dPrV mitotic progenitor into vPrV barrelette neuron subtype identity.

Maintenance of *Hoxa2* Silencing in Postmitotic dPrV Neurons Requires Epigenetic Repression by *Ezh2*

Hoxa2 expression is normally switched off and maintained silenced only in dPrV, but not vPrV, postmitotic neurons (Figures S1A–S1L). To gain insights into the mechanism of maintenance of repression at the *Hoxa2* locus in dPrV neurons, we analyzed the potential involvement of the histone methyltransferase *Ezh2*, a member of the Polycomb Repressive Complex 2 (PRC2), which is involved in epigenetic maintenance of gene silencing by trimethylation of histone H3 at Lysine 27 (H3K27me3) (reviewed in Margueron and Reinberg, 2011).

To generate a conditional *Ezh2* knockout in r2 derivatives, including dPrV neurons, we crossed the *r2::Cre* with a floxed *Ezh2* allele (Puschendorf et al., 2008) and *ROSA::(lox-stop-lox) ZsGreen* to trace neurons and their projections (referred to as $r2^{Ezh2cKO;ZsGreen}$). In E16.5 $r2^{ZsGreen}$ control fetuses, the *Ezh2*-dependent H3K27m3 repressive mark was readily detected by antibody immunostaining both in dPrV and vPrV (Figures 7A–7C). In contrast, in $r2^{Ezh2cKO;ZsGreen}$ mutants (n = 3), H3K27me3 antibody staining was significantly reduced in dPrV and r2-derived territory (asterisk, Figures 7D–7F). In P7 $r2^{Ezh2cKO;ZsGreen}$ mutants, dextran-labeled single whisker (C2) afferent inputs (Figure 7G) were ectopically attracted to dPrV (compare Figures 7H and 7I), similar to $r2^{Hoxa2\text{-}IRES\text{-}EGFP}$ mice (Figures 3C and 4D) and spatially clustered, even though with less precision than in $r2^{Hoxa2\text{-}IRES\text{-}EGFP}$ mice. Moreover, $r2^{Ezh2cKO;ZsGreen}$ projections were maintained in barreloid VPM ($VPM^{barreloid}$) and reduced in lower jaw VPM areas (compare Figures 7K, 7J, and 7O), reminiscent of the $r2^{Hoxa2\text{-}IRES\text{-}EGFP}$ and $Drg11^{Hoxa2\text{-}IRES\text{-}EGFP}$ projection patterns (compare Figures 7K, 6M, and 6W).

To address the actual depletion of the H3K27me3 mark at the *Hoxa2* locus in conditional $r2^{Ezh2cKO;ZsGreen}$ mutants, we compared the in vivo distributions of the H3K27me3 repressive mark at the *Hoxa2* promoter by chromatin immunoprecipitation (ChIP) of PrV neurons isolated by dissection and subsequent fluorescence-activated cell sorting (FACS) from E13.5 $r2^{ZsGreen}$ (control dPrV), *Krox20::Cre;ROSA::(lox-stop-lox)ZsGreen* ($r3^{ZsGreen}$) (control vPrV), and $r2^{Ezh2cKO;ZsGreen}$ conditional knockout cells (cKO dPrV) (Figure 7L). The relative H3K27me3 enrichments correlated with the *Hoxa2* transcriptional "on-off" state, namely low H3K27me3 in $r3^{ZsGreen}$ control vPrV as opposed to high H3K27me3 in $r2^{ZsGreen}$ control dPrV cells (Figure 7M). In $r2^{Ezh2cKO;ZsGreen}$ mutant cells, we detected a significant reduction of the H3K27me3 enrichment as compared to $r2^{ZsGreen}$ control dPrV cells, similar to that of $r3^{ZsGreen}$ control vPrV (compare panels in Figure 7M). These changes in chromatin organization at the *Hoxa2* locus in E13.5 $r2^{Ezh2cKO;ZsGreen}$ mutant cells correlated with transcriptional de-repression of *Hoxa2*, showing about 9-fold increase of *Hoxa2* expression in mutant $r2^{Ezh2cKO;ZsGreen}$ versus control $r2^{ZsGreen}$ cells as assessed by qPCR (Figure 7N). Ectopic expression of *Hoxa2* was also readily detected by in situ hybridization in the E12.5 $r2^{Ezh2cKO}$ dPrV (compare Figures S6F and S6H, arrowheads).

How can *Ezh2* contribute to the maintenance of *Hoxa2* silencing in dPrV but not vPrV postmitotic neurons? One possibility could be that *Ezh2* is differentially expressed between dPrV and vPrV progenitors. To this aim, we analyzed the *Ezh2* expression pattern by in situ hybridization. At E12.5, we found alternating higher and lower expression domains of *Ezh2* in the ventricular zone of the rostral hindbrain (Figures S6C and S6D). Moreover, *Ezh2* appeared to display higher expression in the dPrV than in the vPrV progenitor domains, in particular in the area where $Drg11^+$ neurons accumulate just before migration (Figures S6A, S6B, and arrowheads in S6C and S6D). Different *Ezh2* expression levels might contribute to the differences in relative H3K27me3 enrichments at the *Hoxa2* promoter observed in dPrV versus vPrV cells (Figure 7M).

In summary, *Ezh2* has an important role in maintaining *Hoxa2* silencing in dPrV postmitotic neurons and preventing barrelette

(K–R) Examples of retrogradely traced dendrites of P12 dPrV (K and M) or vPrV (O) projection neurons by EnvA-ΔG-mCherry (K and M) or SAD-ΔG-mCherry (O) rabies viral infection in VPM thalamus of $r2^{TVA\text{-}lacZ}$ (K), $r2^{Hoxa2\text{-}IRES\text{-}EGFP;TVA\text{-}lacZ}$ (M), and control (O) animals with their corresponding polar histograms (L, N, and P) showing dendrite symmetry and length. Note similar asymmetrical organization and length of dendrites in (M) and (O). (Q and R) Quantitative analysis of dendrite symmetry index (Q) and length (R). Neurons (13–20) for each condition were traced. Statistical analysis details in Experimental Procedures. dPrV, dorsal principal trigeminal nucleus; vPrV, ventral principal trigeminal nucleus; SpV, spinal trigeminal nucleus.
See also Figures S3 and S4.

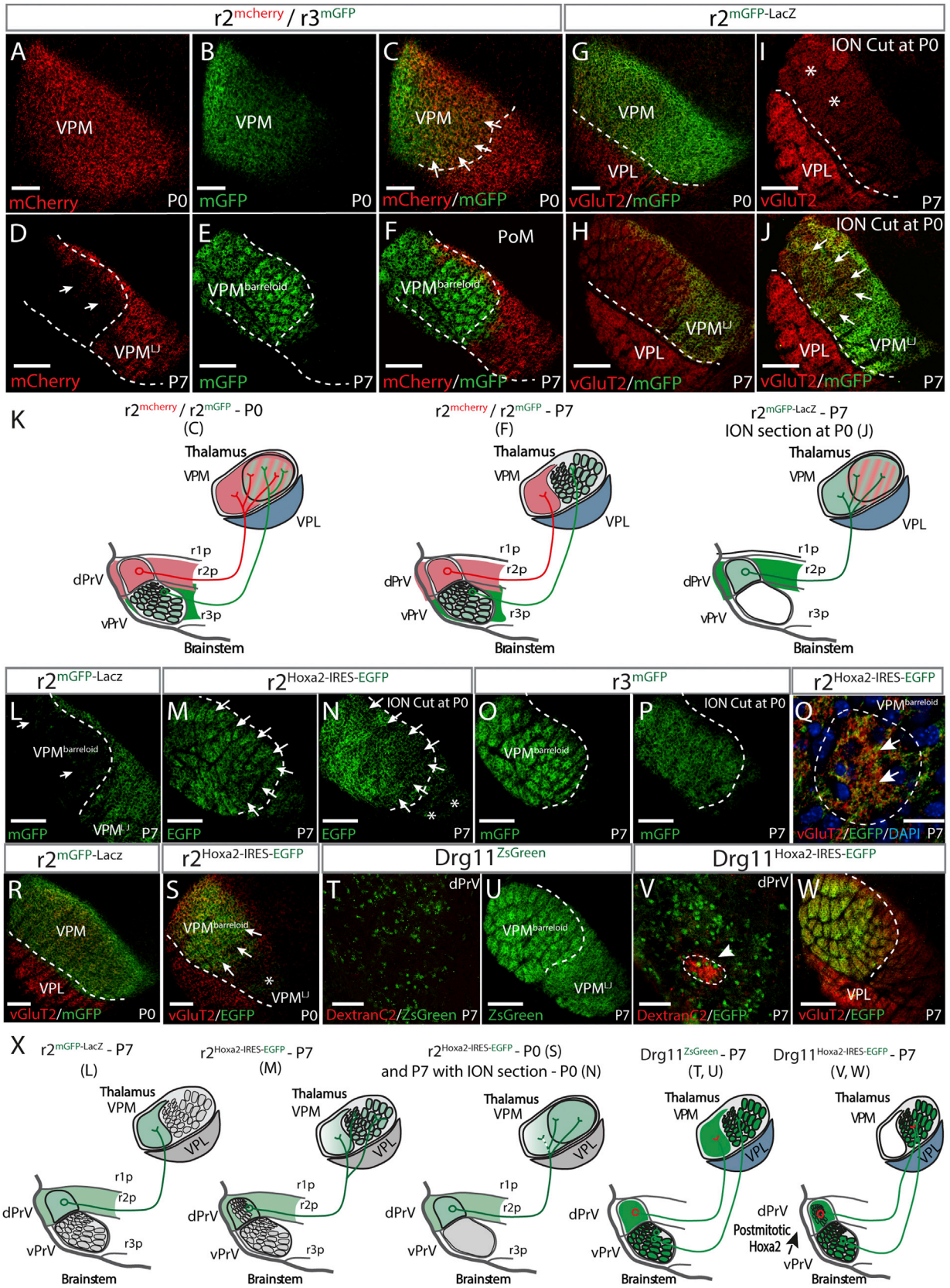

(legend on next page)

circuit formation during facial somatosensory circuit development.

DISCUSSION

Intrinsic versus input-driven molecular mechanisms of somatosensory map formation have been mainly investigated at thalamocortical level (reviewed in O'Leary et al., 2007; Sur and Rubenstein, 2005) whereas little is still known about the molecular control of whisker-related barrelette formation and circuitry. By a genetic gain-of-function approach, we show that the expression of a single HOX transcription factor, HOXA2, in postmitotic dPrV neurons is sufficient to switch dPrV into vPrV barrelette neuron identity and connectivity program (Figure S7).

Ectopic *Hoxa2*-expressing dPrV neurons share several connectivity features with vPrV barrelette neurons. Both the $r2^{Hoxa2\text{-}IRES\text{-}EGFP}$ dPrV and vPrV neurons prenatally target the dorsolateral VPM with topographic precision (Figures 6B and 6S). This is a key step that genetically pre-defines the future barreloid area, unique to vPrV projection neurons, which may be in part achieved by *Hoxa2*-dependent transcriptional regulation of Eph receptor/ephrin ligand family members (Oury et al., 2006). Both the $r2^{Hoxa2\text{-}IRES\text{-}EGFP}$ dPrV and vPrV axon terminals are maintained postnatally in the barreloid area and refined by whisker-dependent activity during barreloid formation (Figures 6E and 6M–6P). At brainstem level, $r2^{Hoxa2\text{-}IRES\text{-}EGFP}$ dPrV neurons are able to attract whisker-related input in a topographic manner, induce expression of factors involved in dendrite orientation (e.g., *Btdb3*) and generate asymmetric dendrite arbors, and allow activity-dependent afferent refinement to generate barrelette-like structures, similar to vPrV neurons (Figures 3, 4, and 5).

In $r2^{Hoxa2\text{-}IRES\text{-}EGFP}$ mice, whisker-related afferents did not ectopically target the dPrV before E16.5 (Figures 3L and 3M). The initial topographic targeting of vPrV and dPrV neurons by whisker-related and mandibular nerve collaterals, respectively, occurred normally (Figures 3J and 3K). This indicates that the ability of *Hoxa2*-overexpressing dPrV neurons to ectopically attract whisker afferents may require temporal accumulation of HOXA2 in postmitotic neurons, in order to override initial dPrV progenitor specification. Recent studies have shown that postmitotic neurons can be reprogrammed in vivo (De la Rossa et al., 2013; Rouaux and Arlotta, 2013). In this respect, we further show that in $Drg11^{Hoxa2\text{-}IRES\text{-}EGFP}$ mice the only expression of *Hoxa2* in postmitotic $Drg11^{+}$ neurons is sufficient to select in dPrV neurons a vPrV-like barrelette-specific input-output connectivity program.

Moreover, as inferred by the *Hoxa2* expression pattern and molecular and anatomical analyses in $r2^{Ezh2cKO}$ mutants (Figures 7, S1, and S6), maintenance of Polycomb-dependent epigenetic repression at the *Hoxa2* locus in postmitotic dPrV neurons prevents barrelette formation and whisker-related circuitry, allowing mandibular sensory circuit development. While the elucidation of the underlying mechanism will require further analysis, our results suggest that differential *Ezh2*-dependent silencing of target genes in dPrV versus vPrV neurons might be in part due to distinct *Ezh2* expression levels in the two progenitor populations. In this respect, it is noteworthy that *Hox* expression patterns have been shown to be sensitive to absolute activity levels of the PRC1 component BMI1 during motor neuron specification (Golden and Dasen, 2012).

Hoxa2-dependent vPrV specification and topographically directed axon targeting of dorsal VPM also provide a necessary template for barreloid formation. In fact, unlike in PrV, where mandibular and whisker-related peripheral inputs are spatially segregated from the outset (Oury et al., 2006), we found that the prenatal thalamic barreloid area receives overlapping inputs from dPrV and vPrV axons. Furthermore, a lesion of the ION affects both the refinement of vPrV inputs and the pruning of dPrV inputs. Thus, ION-mediated activity and/or retrograde molecular signaling from periphery is (are) required for large-scale thalamic somatotopic refinement, which removes most of the non-vPrV projections from the vPrV-targeted perspective barreloid area. Residual non-vPrV axon terminals may be then cleared from the barreloid area through late phases of synaptic elimination (Takeuchi et al., 2014). It will be interesting to investigate the impact of this competition between vPrV and non-vPrV projections on the whisker activity-dependent critical period of barreloid map formation.

In the motor system, *Hox* genes confer diversity of motoneuron subtype identities necessary for fine discrimination of

Figure 6. Perinatal Large-Scale Pruning of Mandibular dPrV Axons in the Thalamic Barreloid Area Is Prevented in *Hoxa2*-Expressing dPrV Neurons

(A–K) Ventral posterior medial (VPM) thalamus coronal sections showing dorsal PrV (dPrV) and/or ventral PrV (vPrV) axon terminal projections at P0 (A–C and G) and P7 (D–F and H–J) in $r2^{mCherry}/r3^{mGFP}$ (A–F) and $r2^{mGFP\text{-}LacZ}$ (G–J) mice. At P0, r2 axons (red) target the whole VPM (A) and overlap r3 projections (green) (C), which are restricted to the future barreloid area ($VPM^{barreloid}$) (B). At P7, r2 and r3 projections are segregated (D–F). Following infraorbital (ION) nerve lesion at P0 (I), barreloids are not formed (asterisks, vGluT2 immunostaining) and r2 projections to the barreloid area are not pruned (arrows) (J). (K) Summary drawings of findings in (A)–(J). Legends refer to experimental panels. Scale bars, 100 μm (A–C and G), 200 μm (D–F and H–J).

(L–P, R, and S) VPM thalamus coronal sections showing dPrV or vPrV axon terminals at P7 (L, M, and O) and P0 (R and S) in $r2^{mGFP\text{-}LacZ}$ (L and R), $r3^{mGFP}$ (O), and $r2^{Hoxa2\text{-}IRES\text{-}EGFP}$ (M and S). Similar to vPrV terminals (B), axons from *Hoxa2*-expressing r2-derived dPrV neurons are topographically directed to the future barreloid area at P0 (S), with little contribution to ventromedial VPM lower jaw area (VPM^{LJ}), and segregate into barreloids (arrows, M) unless infraorbital (ION) nerve lesioning at P0 (N), similar to vPrV projections (P). Scale bars, 200 μm (L–P), 100 μm (R and S).

(Q) $vGluT2^{+}/EGFP^{+}$ and $vGluT2^{+}/EGFP^{-}$ presynaptic axon terminals in single barreloids of P7 $r2^{Hoxa2\text{-}IRES\text{-}EGFP}$ VPM. Scale bar, 25 μm.

(T and V) C2 dextran-labeled afferents (red) ectopically innervate dPrV of P7 $Drg11^{Hoxa2\text{-}IRES\text{-}EGFP}$ animals (V), segregating in a barrelette-like cluster, unlike in control $Drg11^{ZsGreen}$ (T). Scale bars, 50 μm.

(U and W) P7 VPM thalamus coronal sections showing axon projections from trigeminal brainstem nuclei of $Drg11^{ZsGreen}$ (U) and $Drg11^{Hoxa2\text{-}IRES\text{-}EGFP}$ (W). In (W), axonal terminals are restricted to the barreloid area ($VPM^{barreloid}$) unlike in (U). Scale bars, 200 μm.

(X) Summary drawings of findings in (L)–(N), (S), and (T)–(W). Legends refer to experimental panels. VPL, ventral posterior lateral nucleus; PoM, posterior medial nucleus. r1p–r3p, rhombomere 1–3-derived progeny.

See also Figure S5.

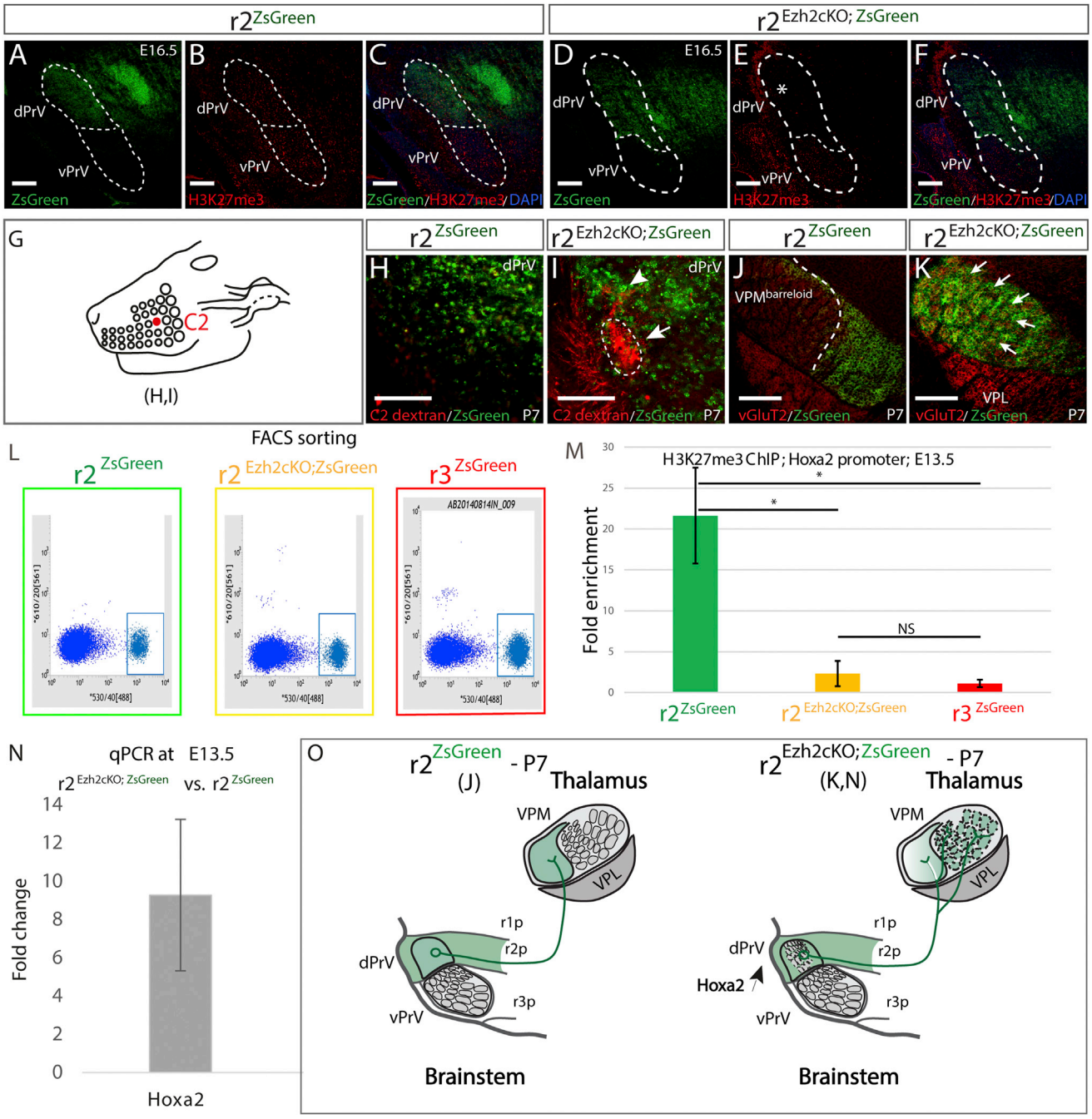

Figure 7. Silencing of *Hoxa2* in Postmitotic dPrV Neurons Requires Epigenetic Repression by *Ezh2*

(A–F) Coronal sections through E16.5 PrV of $r2^{ZsGreen}$ and $r2^{Ezh2cKO;ZsGreen}$ fetuses. Anti-H3K27me3 immunostaining (B and E) showing strong reduction of this mark in $r2^{Ezh2cKO;ZsGreen}$ (asterisk, E) upon *Ezh2* deletion in the r2-derived domain including dPrV. ZsGreen staining identifies r2-derived territory in (A), (C), (D), and (F). Scale bars, 100 μm.

(G) Drawing illustrating dextran injection site to label C2 whisker (red) afferents.

(H and I) C2 dextran-labeled afferents (red) ectopically innervate dPrV of P7 $r2^{Ezh2cKO;ZsGreen}$ (I) as compared to control $r2^{ZsGreen}$ (H). The input segregates in barrelette-like clusters (dashed circles and arrows). Note that targeting precision of C2 afferents is lower in (I) than in Figures 2M and 3C. In (H) and (I), anti-ZsGreen staining identifies r2-derived dPrV cells. Scale bars, 100 μm.

(J and K) dPrV projections are maintained in barreloid VPM (arrows) and reduced in lower jaw VPM areas in $r2^{Ezh2cKO;ZsGreen}$ (K) as compared to control $r2^{ZsGreen}$ (J). Scale bars, 200 μm.

(L and M) Representative FACS profiles of $ZsGreen^{+}$ isolated cells from E13.5 $r2^{ZsGreen}$, $r2^{Ezh2cKO;ZsGreen}$, and $r3^{ZsGreen}$ brains. Blue rectangles in the three panels identify the sorted populations. (M) Profiles of the repressive *Ezh2*-dependent H3K27me3 mark obtained by ChIP of the *Hoxa2* promoter carried out on the

(legend continued on next page)

muscle-specific innervation (Dasen and Jessell, 2009; Philippidou and Dasen, 2013), whereas less information is available about *Hox*-dependent organization of premotor input (Sürmeli et al., 2011). In the somatosensory trigeminal brainstem, *Hoxa2* selects barrelette neuron identity in PrV nucleus and orchestrates the input-output connectivity of a dermatome-specific (i.e., maxillary) circuit module ultimately relaying whisker-related perception from periphery to brainstem to thalamus. Expression of *Hoxa2* is sufficient for topographic coordination of whisker-specific afferent and efferent connectivity of PrV neuron subsets and establishment of whisker-related barrelette pattern. While studies in the last years have identified neuronal molecular distinctions in brainstem and spinal cord related to somatosensory modality or laminar position, the HOXA2 transcription factor is required to organize a somatosensory sub-circuit representing a specific skin receptor area (dermatome). In this respect, HOX factors may be key organizers of regional diversification of sub-circuits underlying the assembly of a functional somatotopic body map.

EXPERIMENTAL PROCEDURES

Animals

All animal procedures were performed in accordance with institutional guidelines and were approved by the Veterinary Department of the Canton of Basel-Stadt.

Generation of Mouse Lines

To generate the *Drg11::Cre* line, the BAC clone RP23-177H12 (BACPAC Resources Center at Children's Hospital Oakland Research Institute, Oakland, CA) containing the entire *Drg11* gene was used as a template for bacterial recombination. Correct recombination and removal of the resistance gene in the *Drg11::Cre* BAC were tested by PCR, restriction enzyme digestion and sequencing. After microinjection into the pronuclei of mouse zygotes, two founders were obtained that displayed the expected *Cre* expression pattern. One founder was used for the study. To generate the *r2::mCherry* line, a mCherry cassette (Clontech) was used to generate a pKS-β-globin-mCherry plasmid. The BamH1 2.5 kb rhombomere 2-specific enhancer of *Hoxa2* (Frasch et al., 1995) was then cloned in reverse orientation 5′ of the β-globin promoter, thus generating a final construct consisting of the r2-specific enhancer, a β-globin minimal promoter, and *mCherry* encoding sequence. The construct was linearized, purified, and microinjected into the pronuclei of mouse zygotes. Founders were identified by PCR. One founder was used for the study. Due to the progressive loss of *Cre* expression after many generations of crossings of a previous *r2::Cre* line (Ren et al., 2002), the original *r2::Cre* DNA construct was reinjected into the pronuclei of mouse zygotes. Two new founders were generated and selected to have a similar r2-specific expression pattern as the previous transgenic *r2::Cre* line. One founder was used for the study. The *Ezh2*$^{fl/fl}$ (Puschendorf et al., 2008) (a kind gift from S.H. Orkin), *LSL-R26Tva-lacZ* (Seidler et al., 2008) (a kind gift from D. Saur), *Tau(lox- stop-lox)mGFP-IRES-NLSlacZ* (Hippenmeyer et al., 2005) (a kind gift from S. Arber), *Hoxa2*$^{EGFP(lox–neo–lox)}$ (Pasqualetti et al., 2002), *ROSA::(lox-stop-lox)Hoxa2-IRES-GFP* (Miguez et al., 2012), and *Krox20::Cre* (Voiculescu et al., 2000) lines were as described. *R26RlacZ* (Soriano, 1999) and *R26RZsGreen* mice were obtained from Jackson Laboratory.

Histological Analysis, Immunostaining, and In Situ Hybridization

Prenatal or postnatal brains, dissected when necessary, were fixed in 4% PFA diluted in PBS for 30 min to overnight. For cryostat coronal sections (25 μm), tissues were cryoprotected in 10% sucrose/PBS and embedded in 7.5% gelatin/10% sucrose/PBS and then frozen at −80°C. Vibratome sections (60 μm, or 30 μm for 3D reconstruction) were prepared from postnatal brains after embedding in 4% agarose/0.1 M PBS (pH 7.4). Immunohistochemistry was as described (Di Meglio et al., 2013). Sections were incubated overnight at 4°C with primary antibodies anti-VGluT2 (1:2,000, Millipore, AB2251), anti-GFP (1:1,000), anti-RFP (1:1,000), anti-H3K27m3 (1:400), rinsed three times in PBS and incubated for 60–90 min at room temperature with Alexa Fluor 488- and/or 546-conjugated secondary antibodies (1:1,000, Invitrogen). Nuclei were stained with DAPI (Invitrogen). In situ hybridization on coronal cryostat sections was as described (Di Meglio et al., 2013). The following probes were used: *Drg11*, *Hoxa2, Hoxb2, Ezh2*, and *Btbd3* (a kind gift of T. Shimogori). Figure S1 is an inverted artificial superposition of chromogenic signals from adjacent sections.

Imaging and Picture Processing

Imaging of fluorescent signals was performed using an Axio imager Z2 upright microscope coupled to a LSM700 Zeiss laser scanning confocal 5× lens (NA 0.25), 10× lens (NA 0.45), or oil/glycerol/water immersion lens 25× (NA 0.8). Chromogenic staining was examined by classical wide-field or binocular microscopy (Nikon).

Dextran Labeling of Single Whisker and Mandibular Afferents

Tetramethyl rhodamine (D3308) or Alexa488 (D3306) conjugated lysine-fixable dextrans (Invitrogen) were used for retrograde labeling of trigeminal nerve branches in pups at day P3. Pups were anesthetized on ice, dextran crystals were directly injected into a given whisker follicle or into lower jaw to label mandibular afferents. After recovery at 37°C, pups were put back with their mother for 4 days allowing dextran diffusion. Vibratome coronal sections (60 μm, or 30 μm for 3D reconstruction) were collected and analyzed under confocal microscope (LSM700).

NeuroVue Dye-Coated Filter Axonal Tracing

NV Red (FS-1002) and NV Maroon (FS-1001) NeuroVue dye-coated filters (Jensen-Smith et al., 2007) were from Molecular Targeting Technologies. Staged fetuses were fixed with 4% PFA/PBS overnight at 4°C. To label mandibular and maxillary afferents to PrV nucleus tiny pieces of NeuroVue filter dyes were placed on the whisker pad row E/D (red) and lower jaw (Maroon: green). To label the dPrV and vPrV projections to the VPM thalamus, P7 pups were perfused with 4% PFA/PBS, brains were dissected and embedded into 4% agarose, and vibratome sections were made starting from the caudal brainstem until the PrV nucleus was apparent. NeuroVue dye filter small pieces were put in dPrV (Maroon: green) and vPrV (red) for simultaneous tracing of their respective axon projections. Brains were incubated at 37°C in 4% PFA/PBS for 4 weeks (E14.5) or 6 weeks (E16.5 and P7) and then cut. Vibratome sections (60 μm) were collected on slides, rapidly mounted in Aqua-Polymount (Polysciences) avoiding dehydration of the tissue and directly imaged under confocal microscope (LSM700).

3D Reconstruction of Tissue Section

Consecutive 30-μm sections of GFP immunostaining from *r2*^{mGFP} or *r2*$^{Hoxa2\text{-}IRES\text{-}EGFP}$ P7 brainstem with dextran-labeled C2 whisker afferent input (red) were imaged with LSM700 confocal microscope. Consecutive images were aligned using Fiji software (manual alignment). Labeled areas and inputs were transformed into surfaces in Bitplane Imaris v7.5.2.6.

Quantification of Mandibular Input Targeted Area in dPrV

The dPrV area targeted by dextran-labeled mandibular afferents was quantified on P7 *r2*$^{mGFP\text{-}LacZ}$ (n = 4) and *r2*$^{Hoxa2\text{-}IRES\text{-}EGFP;mGFP\text{-}LacZ}$ (n = 4) coronal sections using the Fiji software. Values were normalized to the targeted surface area in *r2*$^{mGFP\text{-}LacZ}$ dPrV; the graphs of Figure 3H are presented as the mean ± SD. Statistical analysis was done using non-paired t test (*** $p < 0.0001$).

Infraorbital Nerve Lesions

Infraorbital (ION) nerve lesions were as described (Waite and Cragg, 1982). Briefly, P0 pups were anesthetized by hypothermia on ice for 3 min. For ION resection, a unilateral skin incision was made between the eye and the caudal

isolated cell populations described in (L). H3K27me3 enrichment in *r2*$^{Ezh2cKO;ZsGreen}$ (orange) is significantly reduced, as compared to that of *r2*^{ZsGreen} (green) and similar to that of *r3*^{ZsGreen} (red). Data are represented as mean ± SEM (n = 3).

(N) qPCR showing fold change of *Hoxa2* expression in ZsGreen^{+} from E13.5 cell-sorted *r2*$^{Ezh2cKO;ZsGreen}$ versus *r2*^{ZsGreen} cells.

(O) Summary drawing of findings in (J), (K), and (N). r1p–r3p, rhombomere 1–3-derived progeny. VPL, ventral posterior lateral nucleus; VPM, ventral posterior medial nucleus.

See also Figure S6.

edge of the right whisker pad. The ION was cut with sterile microscissors. Incisions were very small and did not need suture. Pups were then warmed up to 37°C on a heating pad, before being returned to the mother. The entire procedure takes ~5 min. Mice were allowed to recover and daily checked for up to 7 days, before being anaesthetized and perfused for analysis.

TVA/EnvA Viral Tracing and PrV Neuron Dendrite Analysis

EnvA-pseudotyped G-deleted mCherry rabies virus was stereotaxically injected (Kopf Instruments) into P8 $r2^{TVA\text{-}lacZ}$ VPM (from Bregma: 1.6 mm posterior, 1.6 mm lateral, and 3–3.7 mm ventral). A small craniotomy was performed and a pulled-glass pipettes were used for local infusion of the virus by multiple short pulses using a picospritzer (Parker). To trace vPrV barrelette neurons, we performed stereotaxic injections of SAD-ΔG-mCherry (a kind gift of E. Callaway) rabies virus in P8 wild-type mice (same coordinates as above). For all experiments, mice were sacrificed 4 days later, perfused with 4% PFA, and 60-μm vibratome brain sections collected. For each condition, n = 13–20 neurons were traced. Confocal imaging was performed with 40× objective (Zeiss microscope). Arbors were traced using Neurolucida software (MBF Bioscience). Polar histograms with 36 bins of 10° were calculated by summing the length of the processes growing into each bin direction, also taking into account the length in z axis. Values were exported to Microsoft Excel and analyzed. For each dendritic arbor, its zero angle (i.e., the angle in which the dendrites extend the least) was determined automatically by finding an angle in which the vector sum over the semi-circle (+/−90°) was minimal. The symmetry of each dendrite was quantified in reference to this zero angle: this symmetry index (SI) measure was calculated by dividing the summed lengths in the zero-angle direction ± 85° by the summed lengths of dendrites oriented into the opposite directions. An SI of 0 is asymmetric and SI of 1 is uniform. Statistical tests were calculated in MATLAB 2013b with the statistics toolbox. Post hoc Kruskal-Wallis tests were performed for all groups for lengths ($p = 3.5 \times 10^{-06}$) and symmetry measurements ($p = 3.2 \times 10^{-07}$). To compare pairwise between the three groups Wilcoxon rank-sum tests were performed for length and symmetry. The significance level was Bonferroni-corrected ($\alpha = 0.05$) and accepted at ($p < 0.008$).

Chromatin Immunoprecipitation and qPCR

PrV-dissected ZsGreen+ cells from E13.5 $r2^{ZsGreen}$, $r2^{Ezh2cKO;ZsGreen}$, and $r3^{ZsGreen}$ brains were isolated by FACS. Cells were cross-linked for 15 min in 1% PFA/PBS solution and subsequently lysed in cell lysis buffer for 10 min on ice. Nuclei were spun down at 2,500 × *g* for 5 min at 4°C and finally lysed in nuclei lysis buffer. Following 15 min of lysis on a tube shaker at 4°C, samples were sonicated on Covaris and centrifuged at 22,000 × *g* for 15 min at 4°C. Chromatin preparation was diluted 10× with IP dilution buffer and used for IP chromatin preparations, incubated overnight with 2 μg of H3K27me3 antibody (Millipore) on a tube roller at 4°C. Protein G magnetic beads (50 μl) were added and the incubation continued for 2 hr. Beads were washed three times with 1 ml of 0.02% Tween20/TBS solution. Precipitated material was eluted twice for 15 min with 100 μl of 1% SDS/100 mM sodium hydrogen carbonate ($NaHCO_3$) solution at 65°C on a thermal shaker. Twenty microliters of 5 M NaCl was added to the elute and the cross-links reversed by incubating for 6 hr at 65°C. DNA was purified using Min-elute PCR purification kit (QIAGEN). The fold enrichment over input (ΔΔCt) values were calculated using the Ct values of the H3K27me3 enrichment at the *Hoxa2* promoter against an intergenic negative control region that has no H3K27me3 mark, including the respective Ct values of 1% input samples for both regions. The *Hoxa2* promoter PCR amplicon of 113 bp (at −430 bp of the TSS of *Hoxa2*) was amplified with the following primers: forward primer chr6: 52,115,259–52,115,278, CGCCTGCAGTCAT TAACAAA ; reverse primer chr6:52,115,352–52,115,371, TCCCACTCTG CTCCTTTCTC. The negative control PCR amplicon of 142 bp was amplified with the following primers: forward primer chr12: 49,000,661–49,000,680, ATGCCCCTCAGCTATCACAC; reverse primer chr12:49,000,783–49,000,802, GGACAGACATCTGCCAAGGT. For qPCR, $r2^{ZsGreen}$ and $r2^{Ezh2cKO;ZsGreen}$ cells from E13.5 fetuses (n = 2 each genotype) were isolated by FACS and RNA extracted using the Arcturus Pico Pure RNA isolation kit (Applied Biosystems). cDNA was prepared using Superscript III reverse transcriptase system (Life Technologies). QPCR was carried out with StepOne Real Time PCR System (Applied Biosystems). Calculations were done using the delta delta cycle threshold (ddCt) model, using the TATA box binding (TBP) gene as the most suitable reference control (based on the Genevestigator program).

SUPPLEMENTAL INFORMATION

Supplemental Information includes seven figures and can be found with this article online at http://dx.doi.org/10.1016/j.celrep.2015.09.031.

ACKNOWLEDGMENTS

We are grateful to S. Arber, B. Roska, E. Callaway, S.H. Orkin, D. Saur, and T. Shimogori for reagents, viruses, and mouse lines. We thank H. Kohler and FMI facilities for excellent technical assistance. A.B. is the recipient of a EMBO Long-Term Fellowship. Work in F.M.R.'s laboratory is supported by the Swiss National Science Foundation (31003A_149573), ARSEP, and the Novartis Research Foundation.

Received: April 16, 2015
Revised: July 19, 2015
Accepted: September 9, 2015
Published: October 15, 2015

REFERENCES

Beier, K.T., Samson, M.E., Matsuda, T., and Cepko, C.L. (2011). Conditional expression of the TVA receptor allows clonal analysis of descendents from Cre-expressing progenitor cells. Dev. Biol. *353*, 309–320.

da Silva, S., Hasegawa, H., Scott, A., Zhou, X., Wagner, A.K., Han, B.X., and Wang, F. (2011). Proper formation of whisker barrelettes requires periphery-derived Smad4-dependent TGF-beta signaling. Proc. Natl. Acad. Sci. USA *108*, 3395–3400.

Dasen, J.S., and Jessell, T.M. (2009). Hox networks and the origins of motor neuron diversity. Curr. Top. Dev. Biol. *88*, 169–200.

De la Rossa, A., Bellone, C., Golding, B., Vitali, I., Moss, J., Toni, N., Lüscher, C., and Jabaudon, D. (2013). In vivo reprogramming of circuit connectivity in postmitotic neocortical neurons. Nat. Neurosci. *16*, 193–200.

Di Meglio, T., Kratochwil, C.F., Vilain, N., Loche, A., Vitobello, A., Yonehara, K., Hrycaj, S.M., Roska, B., Peters, A.H., Eichmann, A., et al. (2013). Ezh2 orchestrates topographic migration and connectivity of mouse precerebellar neurons. Science *339*, 204–207.

Ding, Y.Q., Yin, J., Xu, H.M., Jacquin, M.F., and Chen, Z.F. (2003). Formation of whisker-related principal sensory nucleus-based lemniscal pathway requires a paired homeodomain transcription factor, Drg11. J. Neurosci. *23*, 7246–7254.

Erzurumlu, R.S., and Gaspar, P. (2012). Development and critical period plasticity of the barrel cortex. Eur. J. Neurosci. *35*, 1540–1553.

Erzurumlu, R.S., Murakami, Y., and Rijli, F.M. (2010). Mapping the face in the somatosensory brainstem. Nat. Rev. Neurosci. *11*, 252–263.

Frasch, M., Chen, X., and Lufkin, T. (1995). Evolutionary-conserved enhancers direct region-specific expression of the murine Hoxa-1 and Hoxa-2 loci in both mice and Drosophila. Development *121*, 957–974.

Golden, M.G., and Dasen, J.S. (2012). Polycomb repressive complex 1 activities determine the columnar organization of motor neurons. Genes Dev. *26*, 2236–2250.

Hippenmeyer, S., Vrieseling, E., Sigrist, M., Portmann, T., Laengle, C., Ladle, D.R., and Arber, S. (2005). A developmental switch in the response of DRG neurons to ETS transcription factor signaling. PLoS Biol. *3*, e159.

Hodge, L.K., Klassen, M.P., Han, B.X., Yiu, G., Hurrell, J., Howell, A., Rousseau, G., Lemaigre, F., Tessier-Lavigne, M., and Wang, F. (2007). Retrograde BMP signaling regulates trigeminal sensory neuron identities and the formation of precise face maps. Neuron *55*, 572–586.

Jensen-Smith, H., Gray, B., Muirhead, K., Ohlsson-Wilhelm, B., and Fritzsch, B. (2007). Long-distance three-color neuronal tracing in fixed tissue using NeuroVue dyes. Immunol. Invest. *36*, 763–789.

Lee, L.J., Lo, F.S., and Erzurumlu, R.S. (2005). NMDA receptor-dependent regulation of axonal and dendritic branching. J. Neurosci. *25*, 2304–2311.

Ma, P.M., and Woolsey, T.A. (1984). Cytoarchitectonic correlates of the vibrissae in the medullary trigeminal complex of the mouse. Brain Res. *306*, 374–379.

Margueron, R., and Reinberg, D. (2011). The Polycomb complex PRC2 and its mark in life. Nature *469*, 343–349.

Matsui, A., Tran, M., Yoshida, A.C., Kikuchi, S.S., U, M., Ogawa, M., and Shimogori, T. (2013). BTBD3 controls dendrite orientation toward active axons in mammalian neocortex. Science *342*, 1114–1118.

Miguez, A., Ducret, S., Di Meglio, T., Parras, C., Hmidan, H., Haton, C., Sekizar, S., Mannioui, A., Vidal, M., Kerever, A., et al. (2012). Opposing roles for Hoxa2 and Hoxb2 in hindbrain oligodendrocyte patterning. J. Neurosci. *32*, 17172–17185.

O'Leary, D.D., Ruff, N.L., and Dyck, R.H. (1994). Development, critical period plasticity, and adult reorganizations of mammalian somatosensory systems. Curr. Opin. Neurobiol. *4*, 535–544.

O'Leary, D.D., Chou, S.J., and Sahara, S. (2007). Area patterning of the mammalian cortex. Neuron *56*, 252–269.

Osakada, F., and Callaway, E.M. (2013). Design and generation of recombinant rabies virus vectors. Nat. Protoc. *8*, 1583–1601.

Osakada, F., Mori, T., Cetin, A.H., Marshel, J.H., Virgen, B., and Callaway, E.M. (2011). New rabies virus variants for monitoring and manipulating activity and gene expression in defined neural circuits. Neuron *71*, 617–631.

Oury, F., Murakami, Y., Renaud, J.S., Pasqualetti, M., Charnay, P., Ren, S.Y., and Rijli, F.M. (2006). Hoxa2- and rhombomere-dependent development of the mouse facial somatosensory map. Science *313*, 1408–1413.

Ozeki, M., and Tabata, Y. (2002). Promoted growth of murine hair follicles through controlled release of basic fibroblast growth factor. Tissue Eng. *8*, 359–366.

Pasqualetti, M., Ren, S.Y., Poulet, M., LeMeur, M., Dierich, A., and Rijli, F.M. (2002). A Hoxa2 knockin allele that expresses EGFP upon conditional Cre-mediated recombination. Genesis *32*, 109–111.

Philippidou, P., and Dasen, J.S. (2013). Hox genes: choreographers in neural development, architects of circuit organization. Neuron *80*, 12–34.

Pouchelon, G., Frangeul, L., Rijli, F.M., and Jabaudon, D. (2012). Patterning of pre-thalamic somatosensory pathways. Eur. J. Neurosci. *35*, 1533–1539.

Puschendorf, M., Terranova, R., Boutsma, E., Mao, X., Isono, K., Brykczynska, U., Kolb, C., Otte, A.P., Koseki, H., Orkin, S.H., et al. (2008). PRC1 and Suv39h specify parental asymmetry at constitutive heterochromatin in early mouse embryos. Nat. Genet. *40*, 411–420.

Ren, S.Y., Angrand, P.O., and Rijli, F.M. (2002). Targeted insertion results in a rhombomere 2-specific Hoxa2 knockdown and ectopic activation of Hoxa1 expression. Dev. Dyn. *225*, 305–315.

Rouaux, C., and Arlotta, P. (2013). Direct lineage reprogramming of post-mitotic callosal neurons into corticofugal neurons in vivo. Nat. Cell Biol. *15*, 214–221.

Seidler, B., Schmidt, A., Mayr, U., Nakhai, H., Schmid, R.M., Schneider, G., and Saur, D. (2008). A Cre-loxP-based mouse model for conditional somatic gene expression and knockdown in vivo by using avian retroviral vectors. Proc. Natl. Acad. Sci. USA *105*, 10137–10142.

Soriano, P. (1999). Generalized lacZ expression with the ROSA26 Cre reporter strain. Nat. Genet. *21*, 70–71.

Sur, M., and Rubenstein, J.L. (2005). Patterning and plasticity of the cerebral cortex. Science *310*, 805–810.

Sürmeli, G., Akay, T., Ippolito, G.C., Tucker, P.W., and Jessell, T.M. (2011). Patterns of spinal sensory-motor connectivity prescribed by a dorsoventral positional template. Cell *147*, 653–665.

Takeuchi, Y., Asano, H., Katayama, Y., Muragaki, Y., Imoto, K., and Miyata, M. (2014). Large-scale somatotopic refinement via functional synapse elimination in the sensory thalamus of developing mice. J. Neurosci. *34*, 1258–1270.

Van Der Loos, H. (1976). Barreloids in mouse somatosensory thalamus. Neurosci. Lett. *2*, 1–6.

Van der Loos, H., Dörfl, J., and Welker, E. (1984). Variation in pattern of mystacial vibrissae in mice. A quantitative study of ICR stock and several inbred strains. J. Hered. *75*, 326–336.

Voiculescu, O., Charnay, P., and Schneider-Maunoury, S. (2000). Expression pattern of a Krox-20/Cre knock-in allele in the developing hindbrain, bones, and peripheral nervous system. Genesis *26*, 123–126.

Waite, P.M., and Cragg, B.G. (1982). The peripheral and central changes resulting from cutting or crushing the afferent nerve supply to the whiskers. Proc. R. Soc. Lond. B Biol. Sci. *214*, 191–211.

Woolsey, T.A., and Van der Loos, H. (1970). The structural organization of layer IV in the somatosensory region (SI) of mouse cerebral cortex. The description of a cortical field composed of discrete cytoarchitectonic units. Brain Res. *17*, 205–242.